Microgravity Science and Technology (2022) 34: 30
https://doi.org/10.1007/s12217-022-09947-2

Capillary Rise of Liquid in Concentric Annuli Under Microgravity

Shangtong Chen[1,2] · Yi Chen[1,2] · Li Duan[1,2] · Qi Kang[1,2]

Received: 14 March 2021 / Accepted: 31 March 2022 / Published online: 13 May 2022

Abstract
The capillary rise of the liquid in concentric annuli under microgravity is studied here. The influences of the dynamic contact angle between the liquid and the annulus wall, the pressure loss caused by the convection, the viscous resistances in the annulus and the reservoir, and the meniscus curvature of the liquid in the reservoir on the capillary rise are all considered in this paper. The capillary driven flow equation in concentric annuli is derived. On the other hand, the equation can also be expressed as a combination of external forces on the control body in the annulus. Under different conditions the capillary driven flow can be divided into two or three regions according to the development of external forces. Two flow models of capillary driven flows in concentric annuli are proposed. This study has been verified by numerical simulations with the VOF (Volume of Fluid) method.

Keywords Capillary driven flow · Concentric annuli · VOF · *Oh* number · *Re* number

Introduction

The capillary driven flow which is a spontaneous interfacial flow driven by surface tension is an important phenomenon in liquid flows in space, especially in surface tension tanks. In order to manipulate the liquid effectively under microgravity conditions, it has a significant meaning to explore problems in capillary driven flows.

The dynamic process of capillary rise was first presented by Lucus and (Washburn 1921). They used a mechanical balance between the capillary, viscous and gravity forces to describe the behavior of capillary rise and derived the well-known Lucus-Washburn equation. (Concus and Finn et al. 1974) explored the liquid equilibrium interface in a container with internal angles and put forward the famous Concus-Finn condition in 1974. A theory of capillary rise in cylindrical tubes was proposed by (Levine et al. 1976) by precisely considering the capillary force, the viscous force and the convective loss. In 2003, a more comprehensive model of capillary rise in cylinder tubes was presented by Stange et al., and the meniscus reorientation, the dynamic contact angle and the development of capillary flow were explored in their paper. The calculation method of dynamic contact angle improved by (Jiang et al. 1979) has been widely accepted. And it was adopted by (Dreyer et al. 1994) to study the capillary driven flow between parallel plates. An accurate prediction of the liquid flow along interior corners was presented by (Weislogel and Lichter 1998), and that was further extended to interior corners with varying wettability (Weislogel et al. 2005) and rounded interior corners (Chen et al. 2006). In 2008 Higuera et al. (2008) studied the penetration of a wetting liquid in the narrow gap between two vertical plates making a small angle. An iterative procedure was implemented such that the Surface Evolver algorithm could be employed to predict steady-state flows along capillary channels of arbitrary cross-section by (Klatte et al. 2008). Different dimensionless scaling methods for the capillary rise of the liquid in a tube or a porous medium were discussed by (Fries et al. 2009). Daniel (2010) conducted drop tower experiments to explore compound capillary flows in complex containers. Wang et al. (2009, 2010) studied the influences of the initial liquid volume and the dynamic contact angle on the capillary driven flow. The Lattice-Boltzmann method based on field mediators was proposed by Wolf et al. in 2010 to simulate the process of capillary rise between

This article belongs to the Topical Collection: Research Pioneer and Leader of Microgravity Science in China: Dedicated to the 85th Birthday of Academician Wen-Rui Hu

✉ Qi Kang
kq@imech.ac.cn

[1] Key Laboratory of Microgravity, Institute of Mechanics, Chinese Academy of Sciences, Beijing 100190, China

[2] College of Engineering & Science, University of Chinese Academy of Sciences, Beijing 100049, China

parallel plates, and the influence of long-range interactions between the fluid and the solid wall was considered. Bolleddula et al. provided a new analytic solution for flows along planar interior edges in 2010, and then discussed a series of geometries of test cells in which compound capillary flows occur spontaneously and simultaneously on local and global length scales. The governing equation of the capillary driven flow in cylindrical interior corners as well as the approximate analytical solution obtained from the equation were given by (Li et al. 2015). Capillary bridges between a plane and a cylindrical wall were predicted precisely by (Reyssat 2015). In 2018 (Wu et al. 2018) established a comprehensive theoretical model for the study on capillary driven flows along curved interior corners. They discovered that the centrifugal force caused by the curve motion was the decisive factor which made the capillary flow in curved interior corners different from that in straight interior corners. In 2019 (Chen et al. 2019) optimized the structure of PMD in tanks by using theories of capillary flows and performed drop tower experiments and numerical simulations with the VOF method to verify its effect. In 2019, (Cheng et al. 2019) studied capillary flows in tubes with variable diameters, and (Chassagne et al. 2019) studied capillary driven flows in axisymmetric geometries. In 2021 (Chen et al. 2021) studied the capillary rise of the liquid in oval tubes in the microgravity environment and proposed a new flow model in which the entire flow period could be divided into two regions.

Besides, in Bottomley (1974) explored the capillary rise of the liquid between concentric circular tubes instead of concentric annuli. But an exact differential equation to describe the meniscus height vs time was not proposed, and the development of forces was not analyzed either. Results for the capillary rise as a function of the radii of the inner and outer cylinders were presented in his paper.

In this paper, a mathematical model for the process of capillary rise in concentric annuli under microgravity is developed, and the impacts of the dynamic contact angle, the pressure loss, the viscous resistance and the curved liquid surface in the reservoir are discussed. The model has been verified by numerical simulations based on the VOF method. In addition, the differential equation is transformed into an equation which consists of a series of forces. The entire process is divided into different regions in each of which only two dominant forces are equated.

Numerical Simulation

Figure 1 shows a typical 3D mesh model established for numerical simulations performed with the VOF method in Fluent. Instead of a circular cylinder, a horizontal square cylinder is selected as the reservoir. This can greatly reduce the workload of building grid models. The width of the square cylinder is 140 mm and its equivalent radius is 79 mm which

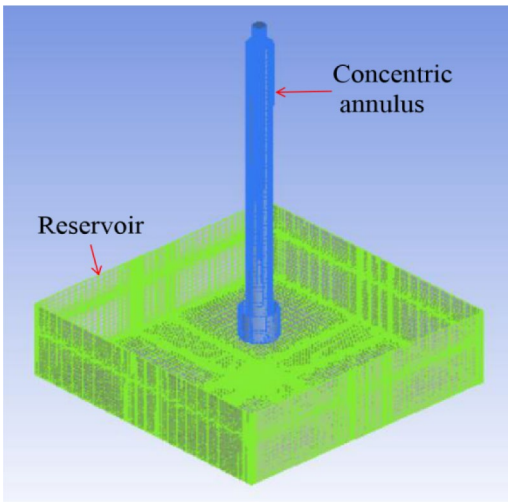

Fig. 1 3D Mesh model of numerical simulation

is used in theoretical calculations. This simplification is accepted, since (according to Fig. 8) the capillary force in the reservoir is quite small compared to other forces and its effects are negligible. The total height of the model is 200 mm. The total number of grids is about 1.2 million. Boundary layers are established near the walls of the reservoir and the annulus. The thickness of the boundary layer at first is about 0.1 mm and its expansion ratio is 1.2. All simulations are conducted twice with a slight difference in boundary layers, and the average of two calculation results is taken as the final result.

Several kinds of Shin-Etsu Silicone Oil KF-96 labeled by their kinematic viscosities (1cSt, 2cSt, 5cSt and 10cSt) are used in our simulations. The properties of different types of silicone oil are listed in Table 1. Numerical settings are listed in Table 2. The calculation process is very stable as the Courant number is much smaller than 1 for most of the calculation time.

A simulation result is shown in Fig. 2. In Fig. 2(a), the red part represents the liquid in the concentric annulus and the reservoir. The liquid is totally at the bottom at first. As the simulation starts, it flows upwards quickly into the annulus and a concave surface is formed at the top of the liquid in the annulus. In Fig. 2(b), the yellow surface represents the gas–liquid interface. The liquid in the annulus, at $t=0$ s, is at the same height as that in the reservoir, and then climbs up and almost reaches the top of the annulus at $t=6$ s.

Table 1 Liquid properties (25 ℃)

Liquid	μ (kg/(m*s))	ρ (kg/m^3)	σ (N/m)	ν (10^{-6} m^2/s)
1cSt	0.000818	818	0.0169	1
2cSt	0.001746	873	0.0183	2
5cSt	0.004575	915	0.0197	5
10cSt	0.00935	935	0.0201	10

Table 2 Numerical Settings

Name	Settings
pressure–velocity coupling equation	SIMPLEC
spatial discretization of the pressure equation	Body Force Weighted
spatial discretization of the gradient equation	Least Square Cell
spatial discretization of the momentum equation	Second-order Upwind Ccheme
spatial discretization of the volume fraction equation	Geo-Reconstruct
relaxation factor	by default

Theoretical Analysis

For theoretical analysis a model is established as shown in Fig. 3. The concentric annulus is immersed into the liquid in the reservoir from above, and the height of the meniscus surface in the annulus is represented by h, therefore, the average velocity of the meniscus is $\dot{h}$. A horizontal cross-section of the annulus is shown in Fig. 4. The inner and outer radii of the annulus are r_i and r_o respectively. The curvature radius of the curved free surface of the liquid inside the reservoir is R_c, which is calculated from the distance c between the wetting barriers and the distance d between the centerline of liquid free surface in the reservoir and the centerline of the annulus. For convenience, the cylindrical coordinate system is selected for the theoretic analysis of this model. The basic assumptions adopted in our analysis include:

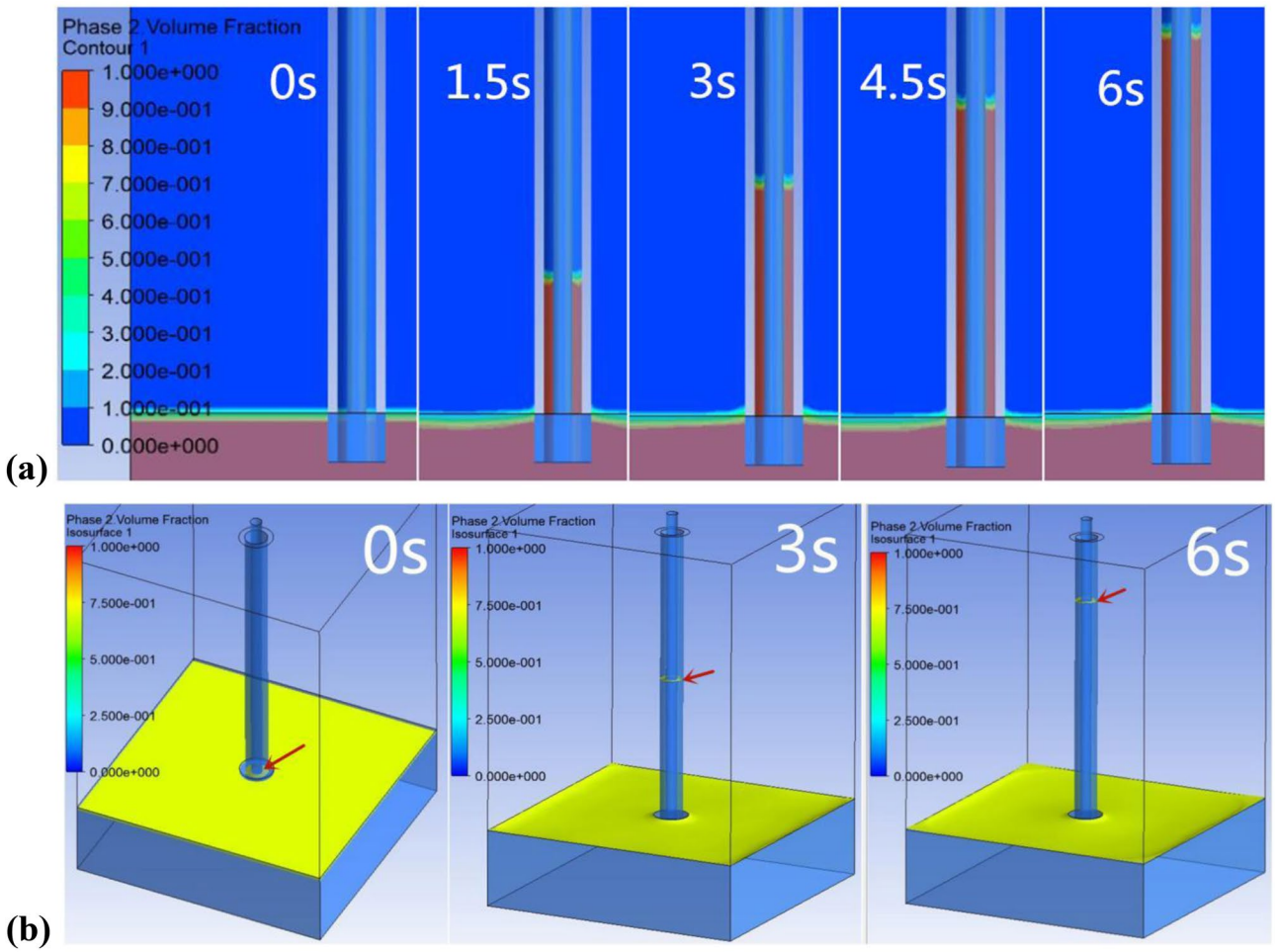

Fig. 2 A numerical result of capillary driven flow with the liquid of 5cSt and $r_i = 3$ mm, $r_o = 6$ mm and $h_0 = 15$ mm. (**a**) Vertical cross section of the numerical model. (**b**) The height of Liquid in the annulus vs time

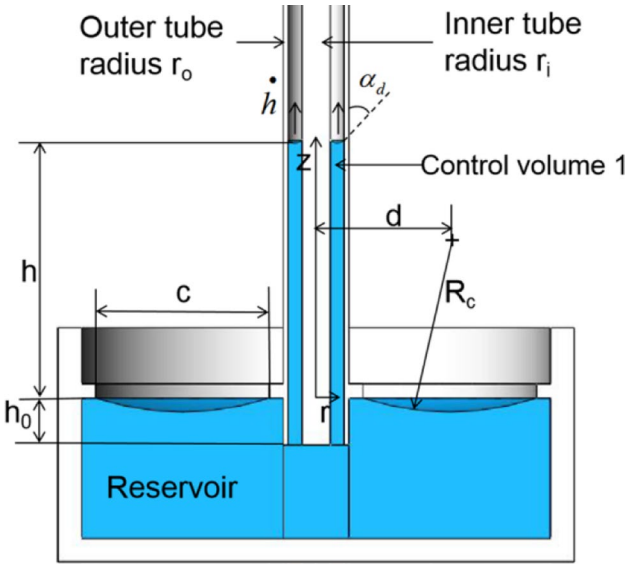

Fig. 3 Front view of the flow in the concentric annulus

(i) No stress acts on the free surfaces.
(ii) The flowing process is isothermal.
(iii) It is fully developed Poiseuille flow.
(iv) The fluid is Newtonian, incompressible and homogeneous.
(v) There is no slip between the flowing liquid and the walls.

From the N-S equation, combined with the boundary conditions, $u|_{r=r_i} = u|_{r=r_o} = 0$, we can obtain the velocity field in a horizontal cross-section of the annulus,

$$u(r,t) = \frac{1}{4\mu}\frac{dp}{dz}r^2 + C_5 \ln r + C_6, r_i \le r \le r_o,$$
$$C_5 = \frac{r_i^2 - r_o^2}{\ln r_o - \ln r_i}\frac{1}{4\mu}\frac{dp}{dz}, C_6 = \frac{r_o^2 \ln r_i - r_i^2 \ln r_o}{\ln r_o - \ln r_i}\frac{1}{4\mu}\frac{dp}{dz} \quad (1)$$

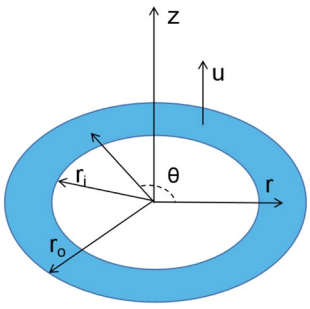

Fig. 4 Horizontal cross-section of the annulus

where μ is liquid's dynamic viscosity. Combined with the volume flux equation, $Q = 2\pi\int_{r_i}^{r_o} urdr = \pi\left(r_o^2 - r_i^2\right)\dot{h}$, Eq. (1) can be transformed into

$$u(r,t) = D\dot{h}\left(r^2 + B\ln r + C\right), r_i \le r \le r_o$$
$$B = \frac{r_i^2 - r_o^2}{\ln r_o - \ln r_i}, C = \frac{r_o^2 \ln r_i - r_i^2 \ln r_o}{\ln r_o - \ln r_i}, D = \frac{1}{\frac{B\left(r_o^2 \ln r_o - r_i^2 \ln r_i\right)}{r_0^2 - r_i^2} + \frac{r_o^2 + r_i^2}{2} - \frac{B}{2} + C} \quad (2)$$

Multiplying the u-component of N-S equation by r, and taking partial derivative with respect to t, we can obtain Eq. (3),

$$\frac{\partial}{\partial t}(ru) = -\frac{r}{\rho}\frac{\partial p}{\partial z} + \nu\left[\frac{\partial}{\partial r}\left(r\frac{\partial u}{\partial r}\right) + r\frac{\partial^2 u}{\partial z^2}\right] \quad (3)$$

where ρ is the liquid density and ν is the kinematic viscosity. By integrating Eq. (3) with respect to r over the entire cross-section of the annulus from $r = r_i$ to $r = r_o$, the following equation can be obtained,

$$\frac{\partial}{\partial t}\int_{r_i}^{r_o} rudr = -\frac{1}{\rho}\int_{r_i}^{r_o} r\frac{\partial p}{\partial z}dr - \nu\left(\left|r_i\frac{\partial u}{\partial r}\right|_{r=r_i}\right| + \left|r_o\frac{\partial u}{\partial r}\right|_{r=r_o}\Bigg|\Bigg) + \nu\frac{\partial^2}{\partial z^2}\int_{r_i}^{r_o} rudr \quad (4)$$

where the velocity filed u is independent of z. Combined with the volume flux equation, Eq. (4) can be written as

$$\frac{1}{2}\left(r_o^2 - r_i^2\right)\ddot{\mathrm{h}} = -\frac{1}{\rho}\int_{r_i}^{r_o} r\frac{\partial p}{\partial z}dr - \nu\left(\left|r_i\frac{\partial u}{\partial r}\right|_{r=r_i}\right| + \left|r_o\frac{\partial u}{\partial r}\right|_{r=r_o}\Bigg|\Bigg) \quad (5)$$

By integrating Eq. (5) with respect to z from $z = -h_0$ to $z = h$ and multiplying it by 2π, we can obtain

$$\pi\left(r_o^2 - r_i^2\right)\left(h + h_0\right)\ddot{\mathrm{h}} = -\frac{2\pi}{\rho}\int_{r_i}^{r_o} r\left[p(h,t) - p\left(-h_0,t\right)\right]dr - 2\pi\nu\int_{-h_0}^{h}\left(\left|r_i\frac{\partial u}{\partial r}\right|_{r=r_i}\right| + \left|r_o\frac{\partial u}{\partial r}\right|_{r=r_o}\Bigg|\Bigg)dz \quad (6)$$

The static contact angle is α_1 between the liquid and the outer tube and α_2 between the liquid and the inner tube, and α_o and α_i are the corresponding dynamic contact angles respectively. The dynamic contact angle increases monotonously with the increases of moving speed of the contact line and the liquid viscosity, and the influence of viscosity is stronger. For a perfectly wetting liquid whose static contact angle is 0°, its dynamic contact angle can be calculated from the formula below.

$$\cos\alpha_d = 1 - 2\tanh\left[4.96 * \left(\frac{\mu\dot{h}}{\sigma}\right)^{0.702}\right] \tag{7}$$

where σ is the surface tension. This equation was proposed in reference (Jiang et al. 1979) and has been widely accepted. For example, it has been adopted to explore the capillary driven flow in cylinder tubes in reference (Stange et al. 2003) and the capillary rise of liquid between parallel plates in reference (Dreyer et al. 1994). When the static contact angle is not 0°, it's going to be more complicated and there is not a uniform formula to predict the dynamic contact angle. However, for a specific liquid, we can measure its dynamic contact angles with the change of speed through experiments and build a formula. The pressure on the upper control surface is

$$\begin{aligned} &p(h,t) = p_0 + p_\sigma \\ &\pi\left(r_o^2 - r_i^2\right)P_\sigma = -2\pi\sigma\left(r_i\cos\alpha_i + r_o\cos\alpha_o\right) \end{aligned} \tag{8}$$

where p_0 is the surrounding air pressure and P_σ is the capillary pressure caused by the curvature of the meniscus.

Furthermore, it is necessary to find another momentum balance on a control volume 2 (CV 2) in the reservoir for calculating the pressure at the inlet. The analysis is based on an equivalent circular entrance, whose radius a equals $\sqrt{r_o^2 - r_i^2}$, as shown in Fig. 5.

Firstly, combined with the mass conservation equation, the force in the z-direction exerting over the hemisphere surface $R = a$ by the fluid in the reservoir outside $R = a$ is

$$\mathrm{x}_1 = \pi a^2\left[\left(p_0 + p_R\right) - \frac{1}{2}\rho a\,\ddot{\mathrm{h}} - \frac{2\mu}{a}\dot{h}\right] \tag{9}$$

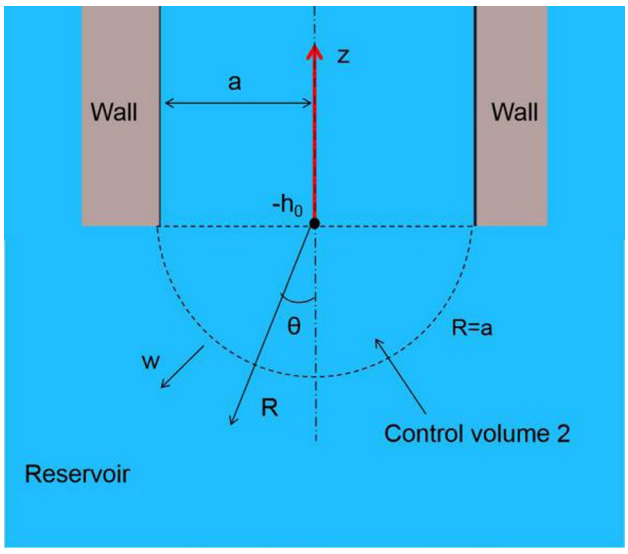

Fig. 5 An equivalent circular entrance and the control volume around the inlet

where is the capillary pressure caused by R_c. According to the geometric relationship, an approximate formula is given for calculating R_c,

$$R_c = -\frac{c^3 d}{6\left(r_o^2 - r_i^2\right)h} \tag{10}$$

$$p_R = \frac{\sigma}{R_c} \tag{11}$$

The force in the z-direction exerting over the circular base $z = -h_0$ by the fluid in the equivalent entrance is

$$\mathrm{x}_2 = -2\pi\int_0^a rp\left(z = -h_0, t\right)dr \tag{12}$$

The flux of momentum in the z-direction entering the hemisphere across $R = a$ is

$$2\pi\rho\mathrm{a}^2\int_0^{\frac{\pi}{2}}\sin\theta w_{R=a}^2\cos\theta d\theta = \frac{1}{4}\pi\rho a^2\dot{h}^2 \tag{13}$$

The flux of momentum leaving at $z = -h_0$ in the z-direction is

$$\begin{aligned} &c2\pi\rho\int \mathrm{ri}^{ro} ru^2 dr = 2\pi E\rho\dot{h}^2 \\ &E = \frac{ro^6 - ri^6}{6} + ro^4\left(\frac{C}{2} - \frac{B}{8} + \frac{B\ln ro}{2}\right) - ri^4\left(\frac{C}{2} - \frac{B}{8} + \frac{B\ln ri}{2}\right) \\ &\quad + ro^2\left[\frac{B^2\left(\ln ro^2\right)}{2} + \frac{B^2}{4} + \frac{C^2}{2} - \frac{BC}{2} - \frac{B\ln ro(B-2C)}{2}\right] \\ &\quad - ri^2\left[\frac{B^2\left(\ln ri^2\right)}{2} + \frac{B^2}{4} + \frac{C^2}{2} - \frac{BC}{2} - \frac{B\ln r_i(B-2C)}{2}\right] \end{aligned} \tag{14}$$

The flux of acceleration in the z-direction inwards $R = a$ is

$$2\pi\mathrm{a}^2\int_0^{\frac{\pi}{2}}\left(\frac{Dw}{Dt}\right)_{R=a}\sin\theta w_{R=a}\cos\theta d\theta = \frac{1}{4}\pi a^2\dot{h}\left(\ddot{\mathrm{h}} + \frac{1}{a}\dot{h}^2\right) \tag{15}$$

The flux of acceleration in the z-direction across $z = -h_0$ is

$$2\pi\int_{\mathrm{r_i}}^{r_o} ru\frac{du}{dt}dr = 2\pi E\dot{h}\ddot{\mathrm{h}} \tag{16}$$

Dividing Eqs. (15) and (16) by the volume flux $\pi a^2\dot{h}$, yield the two accelerations, the average of which is taken as the mean acceleration in the hemisphere. Therefore, the mean acceleration of CV 2 is

$$\frac{2}{3}\pi\mathrm{a}^3\rho\left[\left(\frac{1}{8} + \frac{E}{a^2}\right)\ddot{\mathrm{h}} + \frac{1}{8a}\dot{h}^2\right] \tag{17}$$

In CV 2, we have

$$I_c = I_e - I_l + \Sigma F \tag{18}$$

where I_c stands for the rate of change of total momentum in CV 2, I_e represents the flux of momentum entering CV 2, I_l represents the flux of momentum leaving CV 2, and ΣF stands for the sum of forces acting on CV 2.

Inserting Eqs. (9–17) into Eq. (18), the pressure force at the inlet will be

$$\begin{aligned} x_2 =& \pi a^2 (p_0 + p_R) - 2\pi a\mu\dot{h} - \left(\frac{7}{12} + \frac{2E}{3a^2}\right) \\ & \pi a^3 \rho \ddot{\mathrm{h}} - \left(\frac{2E}{a^2} - \frac{1}{6}\right)\pi a^2 \rho \dot{h}^2 \end{aligned} \tag{19}$$

Inserting Eqs. (2), (7), (8) and (19) into Eq. (6), the differential equation for the height of the meniscus is obtained as below,

$$\begin{aligned} \ddot{\mathrm{h}} =& \frac{1}{h + h_0 + \left(\frac{7}{12} + \frac{2E}{3a^2}\right)a} \left\{ \frac{\sigma}{\rho}\left[\frac{2(r_i \cos\alpha_i + r_o \cos\alpha_o)}{a^2} - \frac{1}{R_c}\right] \right. \\ & \left. - \left[\frac{2|D|F}{a^2}(h + h_0) + \frac{2}{a}\right]\nu\dot{h} - \left(\frac{2E}{a^2} - \frac{1}{6}\right)\dot{h}^2 \right\} \\ & F = r_i \left|2r_i + \frac{B}{r_i}\right| + r_o \left|2r_o + \frac{B}{r_o}\right| \end{aligned} \tag{20}$$

Equation (20) can be solved using the forth order Runge–Kutta method with the initial conditions, $\dot{h}(t = 0) = h(t = 0) = 0$.

Comparison Between Theoretical and Numerical Results

Figure 6 shows the results of meniscus height vs time obtained from theoretical and numerical analyses, where the solid curves are from theoretical analysis and the square signs stand for numerical results. Two pairs of data comparisons between theoretical and numerical results are presented in each Figure. They are identified by being plotted in different colors. It can be seen that numerical results are in good agreement with theoretical results. And the increase in viscosity will significantly slow down the liquid flow rate. Comparing Fig. 6(b), (c), we can see that reducing h_0 is beneficial to increase the liquid flow speed. Their calculation parameters are listed in Table 3.

Discussion

Equation (20) can also be expressed as a sum of forces. The capillary flow can be divided into different time domains in each of which only two forces play the dominant role. With the capillary force in the annulus being the driving force, Eq. (20) can be written as

$$F_{ca} = F_{ia} + F_{ir} + F_{cr} + F_{fa} + F_{fr} + F_{pl} \tag{21}$$

The meanings of the force terms are:

capillary force in the annulus
inertia force in the reservoir $F_{ir} = \rho\pi a^2\left[\left(\frac{7}{12} + \frac{2E}{3a^2}\right)a + h_0\right]\ddot{\mathrm{h}}$
pressure loss force at the entrance
friction force in the annulus $F_{fa} = 2\pi|D|F\mu(h + h_0)\dot{h}$
capillary force in the reservoir $F_{cr} = \frac{6\pi a^4}{c^3 d}\sigma h$
friction force in the reservoir $F_{fr} = 2\pi\mu a\dot{h}$
inertia force in the annulus $F_{ia} = \rho\pi a^2 h\ddot{\mathrm{h}}$

Properties of the Liquids used in this study are shown in Table 1. *Oh* number and *Re* number are used to distinguish flow features in different situations. *Oh* number reflects the relationship between the viscous force, the surface tension force and the inertia force, while *Re* number reflects the relationship between the viscous force and the inertia force. They are calculated from Eqs. (22) and (23) respectively.

$$Oh = \mu/\sqrt{\rho\sigma A} \tag{22}$$

$$\mathrm{Re} = \rho v A/\mu \tag{23}$$

where A is the equivalent diameter of the annulus, which equals $2\sqrt{r_o^2 - r_i^2}$.

In previous studies about capillary driven flows in cylinder tubes, the flow is divided into 3 regions in all cases. It is not very accurate in the case discussed in this paper. The capillary driven flow in concentric annuli is more complicated. The development of external forces vs time in different conditions for the case of high *Oh* number is shown in Fig. 7, where the x-axis is the time t, and the y-axis is the force F. The red, green, cyan, blue and magenta solid curves represent the capillary driven force F_{ca}, the inertia force in the reservoir F_{ir}, the pressure loss in the entrance F_{pl}, the friction force in the annulus F_{fa}, and the capillary force in the reservoir F_{cr}, respectively, and the dashed curve stands for the inertia force in the annulus F_{ia}. The capillary driven force is effective from the beginning and starts with the maximum value. Besides F_{ca}, F_{ir} is the dominant force at the beginning but decreases rapidly. At a certain time, F_{ca} surpasses F_{ir} and plays the dominant role. Other forces are negligible compared to the dominant ones. Approximate solutions can be obtained by equating only two forces in the respective time domains.

The capillary force is always the driving force. Equating the inertia force in the reservoir F_{ir} and the capillary force in the annulus F_{ca}, yields the flow speed in the first region:

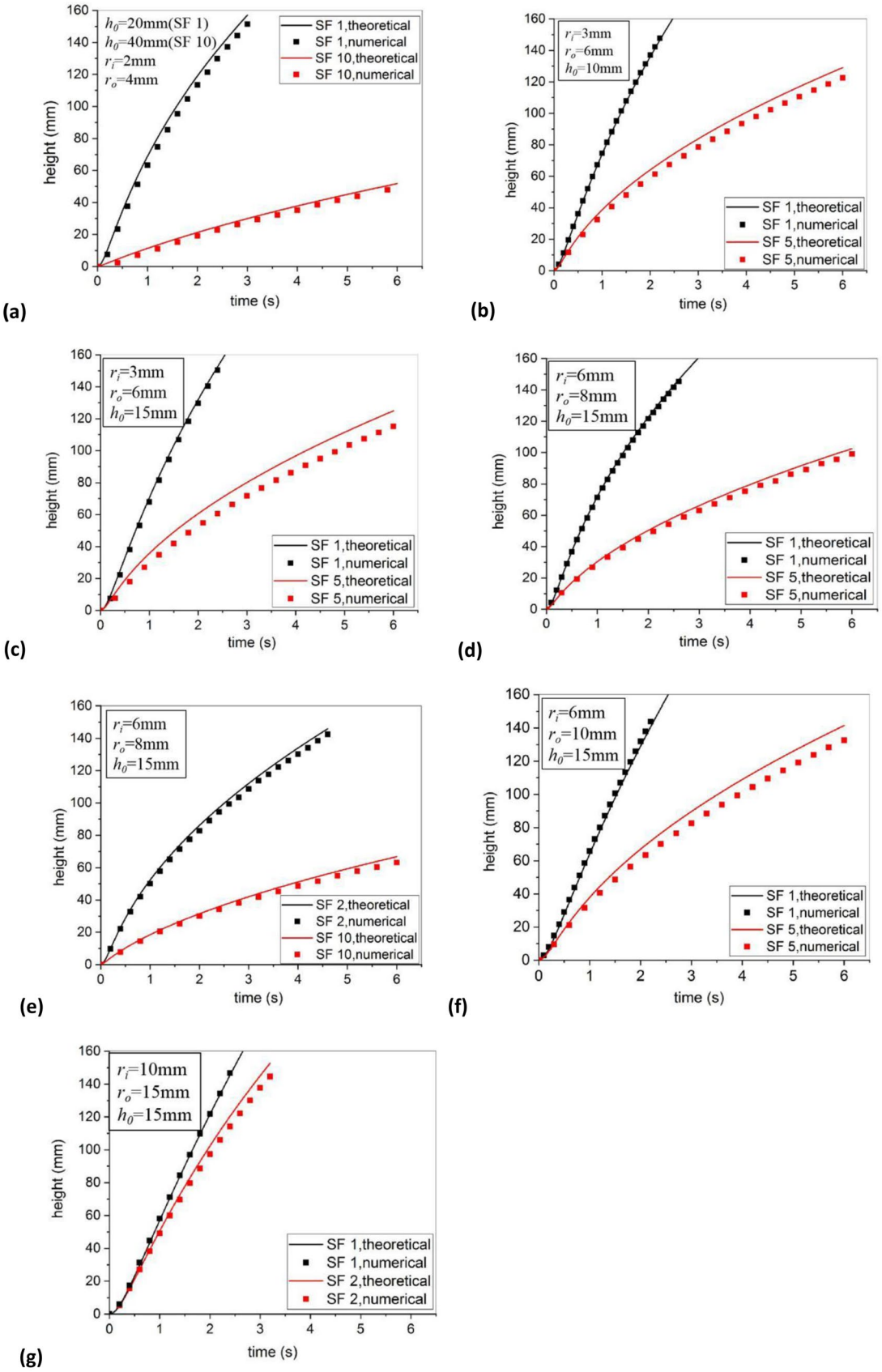

Fig. 6 Comparison between theoretical and numerical results

Table 3 Numerical parameters

No	r_i [mm]	r_o [mm]	h_0 [mm]	Liquid	v_{max} [mm/s]	Re_{max}	t_{1l} [s]	t_{1h} [s]	t_{2l} [s]	Oh 10^{-3}
#1	2	4	20	1cSt	82.3	570	…	…	…	2.64
#2	2	4	40	10cSt	12.6	8.73	…	0.499	…	25.9
#3	3	6	10	1cSt	84.1	874	0.139	…	0.392	2.16
#4	3	6	10	5cSt	49.6	103	…	0.117	…	10.6
#5	3	6	15	1cSt	80.5	837	0.185	…	0.392	2.16
#6	3	6	15	5cSt	44.3	92.1	…	0.140	…	10.6
#7	6	8	15	1cSt	86.8	919	0.150	…	0.173	2.14
#8	6	8	15	2cSt	67.3	356	…	…	…	4.25
#9	6	8	15	5cSt	40.5	85.7	…	0.102	…	10.5
#10	6	8	15	10cSt	23.6	25.0	…	0.110	…	21.0
#11	6	10	15	1cSt	73.9	1182	0.243	…	0.693	1.74
#12	6	10	15	5cSt	44.7	143	…	…	…	8.52
#13	10	15	15	1cSt	68.4	1530	0.307	…	1.08	1.47
#14	10	15	15	2cSt	59.5	665	…	…	…	2.92

$$\dot{h_{1h}}(t) = \frac{F_{ca}}{\rho\pi a^2\left[\left(\frac{7}{12}+\frac{2E}{3a^2}\right)a+h_0\right]}t \tag{24}$$

with the initial condition, $\dot{h}(t=0)=0$. So the meniscus height h in the first region is proportional to t^2. And equating F_{ca} with F_{fa} for the second region, yields

$$h_{2h}(t) = \frac{\sqrt{C_1^2h_0^2+2C_1F_{ca}t}-C_1h_0}{C_1}+C_3, C_1 = 2\pi|D|F\mu \tag{25}$$

where C_3 is a constant. So the velocity in the second region becomes

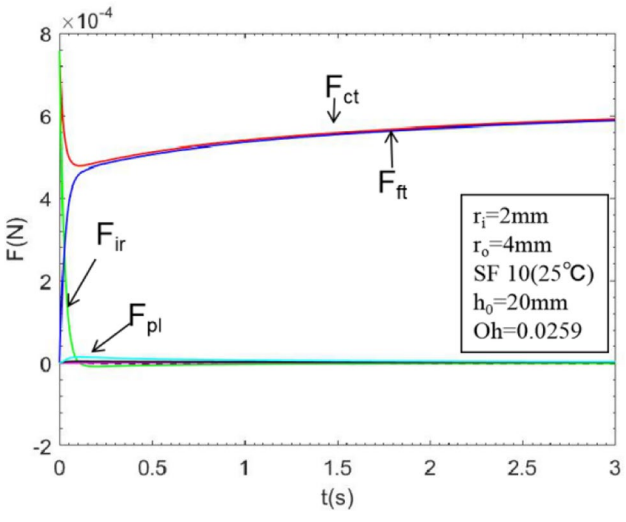

Fig. 7 Development of different forces vs time in 10cSt in the annulus with $r_i = 2$ mm and $r_o = 4$ mm

$$\dot{h_{2h}} = \frac{F_{ca}}{\sqrt{C_1^2h_0^2+2C_1F_{ca}t}} \tag{26}$$

The moment t_{1h}, which demarcates these two regions, can be obtained by equating $\dot{h_{1h}}$ and $\dot{h_{2h}}$, written as

$$t1h = s1+s2,\ s1 = \sqrt[3]{\sqrt{\frac{q^2}{4}+\frac{p^3}{27}}-\frac{q}{2}},\ s2 = \sqrt[3]{-\sqrt{\frac{q^2}{4}+\frac{p^3}{27}}-\frac{q}{2}}$$
$$p = -\frac{C_1^2h_0^4}{12F_{ct}^2},\ q = \frac{C_1^3h_0^6}{108F_{ca}^3}-\frac{C_2^2}{2C_1F_{ca}},\ C_2 = \rho\pi a^2\left[\left(\frac{7}{12}+\frac{2E}{3a^2}\right)\alpha+h_0\right] \tag{27}$$

In the case of low Oh number, the development of forces is more complicated than that in the case of high Oh number, and Re number is also needed to analyze the flow features. The development of forces in 1cSt in 4 kinds of concentric annuli is shown in Fig. 8(a), (b), (c), (d). We can see from the Figures that, when $\mathrm{Re} \le 300$, F_{pl} can be neglected, which means that the flow in this situation can be divided into two regions as that in the case of high Oh number; when $300 \le \mathrm{Re} \le 800$, F_{pl} and F_{ca} are of the same magnitude, and the second region of capillary flow is influenced (dominated?) by F_{ca}, F_{pl} and F_{ca} (F_{ca} repeated? / in sequence?); when $800 < \mathrm{Re} \le 2000$, F_{ir}, F_{pl} and F_{fa} play a leading role respectively in a certain period of time, so the flow can be divided into three regions in this situation. The velocity equation in the first region is the same as that in the case of high Oh number, which is

$$\dot{h_{1l}}(t) = \frac{F_{ca}}{\rho\pi a^2\left[\left(\frac{7}{12}+\frac{2E}{3a^2}\right)a+h_0\right]}t \tag{28}$$

While in the second region, F_{ca} is equated to F_{pl}, which yields

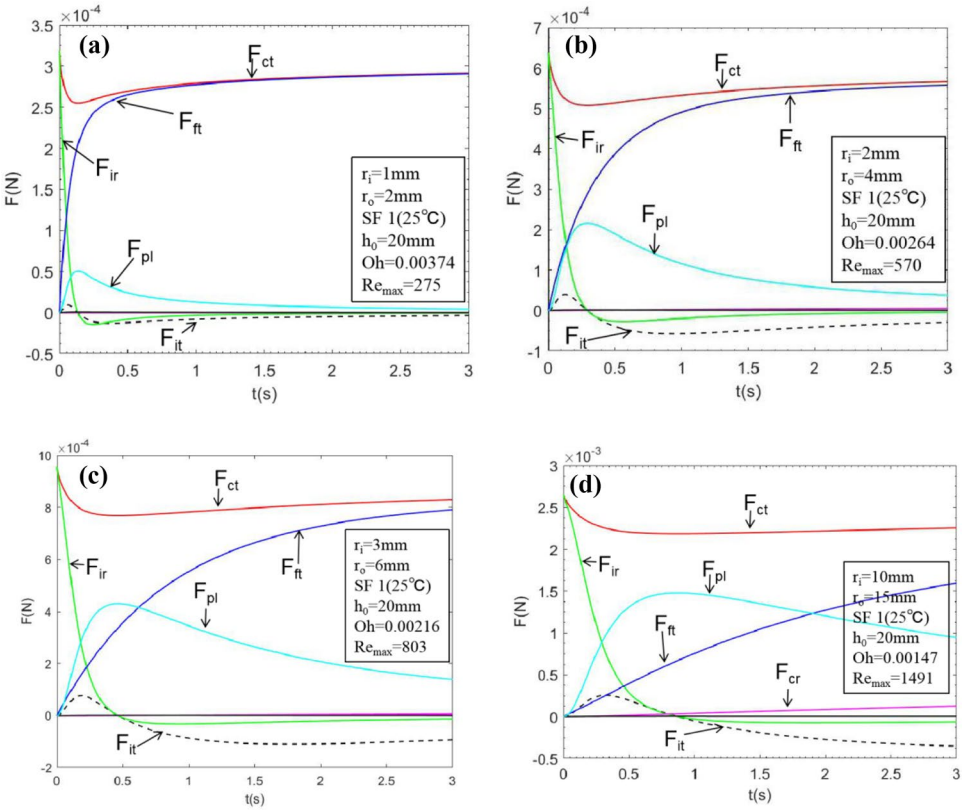

Fig. 8 Development of different forces vs time in 1cSt in different annuli. (**a**) $r_i = 1$ mm and $r_o = 2$ mm; (**b**) $r_i = 2$ mm and $r_o = 4$ mm; (**c**) $r_i = 3$ mm and $r_o = 6$ mm; (**d**) $r_i = 10$ mm and $r_o = 15$ mm

$$\dot{h_{2l}}(t) = \sqrt{\frac{F_{ca}}{\left(\frac{2E}{a^2} - \frac{1}{6}\right)\rho\pi a^2}} \tag{29}$$

The meniscus height h is proportional to the time t in the second region. Time t_{1l} can be obtained from the intersection of the two velocity curves, that is

$$t_{1l} = \left[\left(\frac{7}{12} + \frac{2E}{3a^2}\right)a + h_0\right]\sqrt{\frac{\rho\pi a^2}{\left(\frac{2E}{a^2} - \frac{1}{6}\right)F_{ca}}} \tag{30}$$

In the case of low *Oh* number, the liquid flow speed is much faster and the meniscus height is high enough to neglect h_0. The velocity equation in the third region is written as

$$\dot{h_{3l}}(t) = \sqrt{\frac{F_{c\alpha}}{4\pi|D|F\mu}\frac{1}{\sqrt{t}}} \tag{31}$$

Therefore, h is linearly related to $t^{1/2}$ in the third region. The time at the intersection of the two curves of $\dot{h_{2l}}$ and $\dot{h_{3l}}$ is, $t_{2l} = \left(\frac{2E}{a^2} - \frac{1}{6}\right)\rho a^2/(4|D|F\mu)$.

Besides, Stange et al. has presented in reference Chen et al. (2021) that, if $\Lambda_1 = h_0/r$ is large enough, the capillary flow in cylinder tubes can be divided into two regions. This rule is applicable to concentric annuli as well with the equivalent radius of the annulus, a, taking place of the radius of the cylinder tube, r.

From the velocity equations in different regions, an approximate solution for $h(t)$ can be obtained. Figure 9(a) shows the development of meniscus height vs time in the case of low *Oh* number and high *Re* number. In this situation the capillary flow can be divided into three regions, and the height is proportional to t^2, t and $t^{1/2}$ in Region 1, 2 and 3 respectively. Figure 9(b) shows the development of meniscus height vs time in the case of high *Oh* number or in the case of low *Oh* number and low *Re* number. In this situation, the capillary driven flow is divided into two regions, and for the capillary flow that continues for a long time period, the liquid flow distance is long enough to neglect h_0 and the height is proportional to $t^{1/2}$ in the second region.

Two typical types of capillary driven flow are shown in Fig. 10(a) and (b). According to Table 3, the moments that demarcate different regions are labeled in the Figures. In Fig. 10(a), the *Oh* number is 0.00147 and the *Re* number is 1530. In the first region, the curve of the data is parabolic. In the second region, the data fit a straight line. In order to observe this trend more intuitively, a dashed line that shows the height proportional to t is established starting from t_1. After t_2 the data deviate from the dashed line, because the height is proportional to $\sqrt{t}$ in the third region. In Fig. 10(b), the *Oh* number is 0.021. The region in which the meniscus height is proportional to t doesn't exist any longer, therefore the flow is divided into 2 regions under this condition.

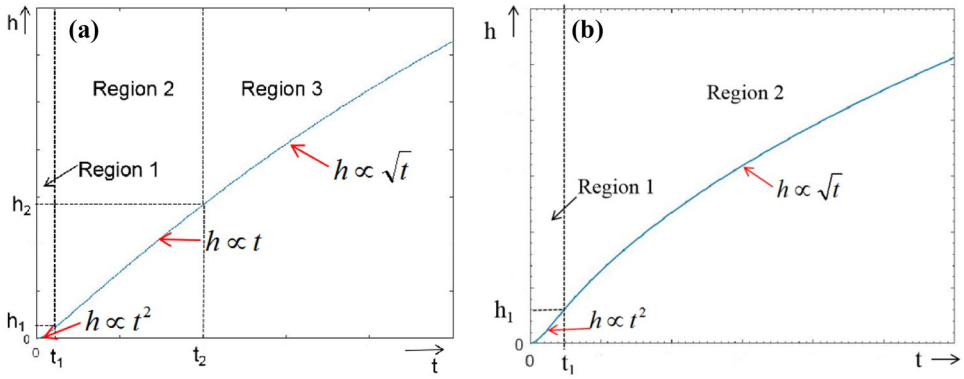

Fig. 9 General representation of capillary rise in concentric annuli. (**a**) Capillary flow in the case of low *Oh* number and high *Re* number; (**b**) capillary flow in the case of high *Oh* number or in the case of low *Oh* number and low *Re* number

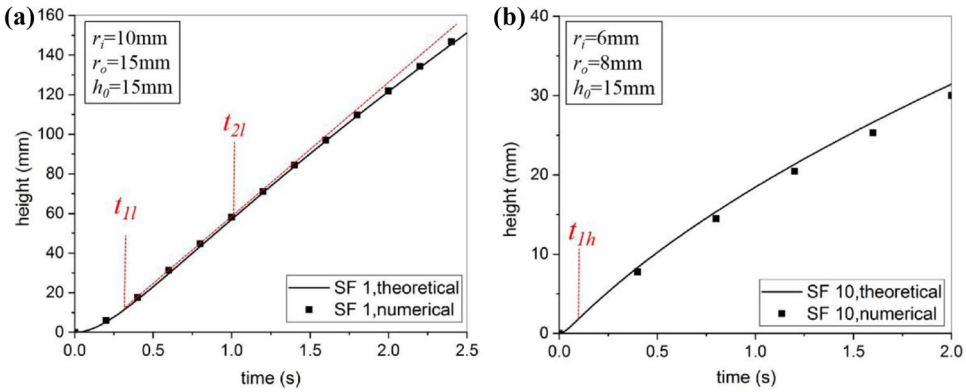

Fig. 10 Two typical capillary driven flows. (**a**) 1cSt in the annulus with $r_i = 10$ mm, $r_o = 15$ mm and $h_0 = 15$ mm; (**b**) 10cSt in the annulus with $r_i = 6$ mm, $r_o = 8$ mm and $h_0 = 15$ mm

Besides, when the gap is narrow enough, the capillary rise in concentric annuli would be quite close to liquid penetration between parallel plates. In this condition we can use the flow equation between parallel plates. This wouldn't cause much error and can simplify calculation procedure. However, even when the gap is wide enough, the capillary rise in concentric annuli wouldn't be similar with liquid penetration in cylinder tubes. Because of the existence of the inner tube, the velocity field in concentric annuli is totally different from that in cylinder tubes.

Summary

An exact equation of capillary rise of liquid in concentric annuli is obtained and verified by numerical simulations with the VOF method. Six sizes of annuli and four types of Silicone oil are used. The theoretical and numerical results are in good agreement. According to this equation, capillary driven flows in concentric annuli under microgravity can be predicted precisely. Two flow models of capillary driven flows in concentric annuli are proposed in this study. Besides, the influences of the dynamic contact angle and the initial liquid height h_0 in the annulus are also considered.

Moreover, an approximate solution by considering simplified forces is presented as well. By considering only two dominant forces at a time, the flows can be divided into two regions or three regions under different conditions. The capillary force is always the driving force and is balanced with the inertia force in the reservoir, the pressure loss in the entrance or the viscous resistance in the annulus in different regions respectively. *Oh* number and *Re* number are both adopted to compare effects of different forces.

The exact equation of meniscus height vs time in concentric annuli under microgravity is derived for the first time. And the development of forces is analyzed comprehensively and different flow features are obtained. The flow process is more complicated than that in cylinder tubes. This can deepen people's understanding of capillary driven flow. The conclusions drawn in this paper will be greatly helpful for liquid management in space, especially for the design of surface tension tanks. And these analytical methods can also be used in capillary driven flows in other circumstances.

Acknowledgements This research was funded by the China Manned Space Engineering Program (Fluid Physics Experimental Rack and the Priority Research Program of Space Station), the Strategic Priority Research Program of Chinese Academy of Sciences (No. XDB23030300) and the Natural Science Foundation Project (No. 12032020, and No. 12072354).

Declarations

Conflicts of Interests The authors declare no competing financial interest.

References

Bottomley, G.A.: The capillary rise between concentric circular tubes. Aust. J. Chem. **27**(11), 2297–2306 (1974)

Chassagne, R., Dörfllfler, F., Guyenot, M., Harting, J.: Modeling of capillary-driven flows in axisymmetric geometries. Comput. Fluids **178**, 132–140 (2019)

Chen, S.-T., Han, Z.-Y., Duan, L., Kang, Q.: Experimental and numerical study on capillary flow along deflectors in plate surface tension tanks in microgravity environment. AIP Advances **9**, 025020 (2019)

Chen, S.-T., Ye, Z.-J,. Duan, L., Kang Q.: Capillary driven flow in oval tubes under microgravity. Phys. Fluids **33**: 032111 (2021)

Chen, Y.-K., Weislogel, M.M., Nardin, C.L.: Capillary driven flows along rounded interior corners. J. Fluid Mech. **556**, 235–271 (2006)

Cheng, X., Chen, Y., Li, H.-R., Li, B.-X., Han, X., Xin, G.-M.: Investigation on capillary flow in tubes with varible diameters. J. Porous Media **22**(13), 1627–1638 (2019)

Concus, P., Finn, R.: On capillary free surfaces in the absence of gravity. Acta Math. **132**, 177–198 (1974)

Daniel, A.B., Chen, Y.-K., Semerjian, B., Tavan, N., Weislogel, M.M.: Compound capillary flows in complex containers: drop tower test results. Microgravity Sci. Technol. **22**, 475–485 (2010)

Dreyer, M., Delgado, A., Rath, H.J.: Capillary rise of liquid between parallel plates under microgravity. J. Colloid Interface Sci. **163**, 158–168 (1994)

Fries, N., Dreyer, M.E.: Dimensionless scaling methods for capillary rise. J. Colloid Interface Sci. **338**(2), 514–518 (2009)

Higuera, F.J., Medina, A., Linan, A.: Capillary rise of a liquid between two vertical plates making a small angle. Phys. Fluids **20**, 102102 (2008)

Jiang, T.-S., Oh, S.-G., Slattery, J.C.: Correlation for dynamic contact angle. J. Colloid Interface Sci. **69**, 74–77 (1979)

Klatte, J., Haake, D., Weislogel, M.M., Dreyer, M.: A fast numerical procedure for steady capillary flow in open channels. Acta Mech. **201**, 269–276 (2008)

Levine, S., Reed, P., Watson, E.J., Neale, G.: A theory of the rate of rise of a liquid in a capillary. J. Colloid Interface Sci. **3**, 403–419 (1976)

Li, Y.-Q., Hu, M.-Z., Liu, L., Su, Y.-Y., Duan, L., Kang, Q.: Study of capillary driven flow in an interior corner of rounded wall under microgravity. Microgravity Sci. Technol. **27**, 193–205 (2015)

Reyssat, E.: Capillary bridges between a plane and a cylindrical wall. J. Fluid Mech. **773**, R1 (2015)

Stange, M., Dreyer, M., Rath, H.: Capillary driven flow in circular cylindrical tubes. Phys. Fluids **15**, 2587–2601 (2003)

Wang, C.-X., Xu, S.-H., Sun, Z.-W., Hu, W.-R.: Influence of contact angle and tube size on capillary-driven flow under microgravity. AIAA J. **47**(11), 2642 (2009)

Wang, C.-X., Xu, S.-H., Sun, Z.-W., Hu, W.-R.: A study of the influence of initial liquid volume on the capillary in interior corner under microgravity. Int. J. Heat Mass Transf. **53**(9–10), 1801 (2010)

Washburn, E.W.: The dynamics of capillary flow. Phys. Rev. **17**, 273–283 (1921)

Weislogel, M.M., Lichter, S.: Capillary flow in an interior corner. J. Fluid Mech. **373**, 349–378 (1998)

Weislogel, M.M., Nardin, C.L.: Capillary driven flow along interior corners formed by planar walls of varying wettability. Microgravity Sci. Technol. **17**(3), 45–55 (2005)

Wolf, F., Santos, L., Phillippi, P.: Capillary rise between plates under dynamic conditions. J. Colloid Interface Sci. **344**, 171–179 (2010)

Wu, Z.-Y, Huang, Y.-Y, Chen, X.-Q., Zhang, X.: Capillary driven flows along curved interior corners. I .J. Multiphase Flow **109,** 14–25 (2018)